catalysts

MDPI

Article

Highly Active Ni–Fe Based Oxide Oxygen Evolution Reaction Electrocatalysts for Alkaline Anion Exchange Membrane Electrolyser

Immanuel Vincent [1,2], Eun-Chong Lee [1] and Hyung-Man Kim [1,*]

[1] Department of Mechanical Engineering, High Safety Vehicle Core Technology Research Center, INJE University, 607 Eobang-Dong, Gimhae-si 621-749, Gyongsangnam-do, Korea; immanuel.vincent@tecnalia.com (I.V.); eunch14@naver.com (E.-C.L.)
[2] TECNALIA, Basque Research and Technology Alliance (BRTA), Mikeletegi Pasealekua 2, 20009 Donostia-San Sebastián, Spain
* Correspondence: mechkhm@inje.ac.kr; Tel.: +82-55-320-3666; Fax: +82-55-324-1723

Abstract: Oxygen evolution reaction (OER) electrocatalysts are pivotal for sustainable hydrogen production through anion exchange membrane electrolysis. Cost-effective transition metals such as nickel and iron-based oxides (Ni–Fe–O_x) have been recognized as viable catalysts for the oxygen evolution process in alkaline media. In this work, we study the electrochemical characterization and stability of the Ni–Fe–O_x to find the suitability for AEM electrolysis. The results indicate that Ni–Fe–O_x has 5 times higher activity than pure Ni. The Ni–Fe–O_x electrodes exhibit an exceptionally high catalytic activity of 22 mA cm^{-2} at 1.55 V vs. RHE, and a Tafel value as low as 97 dec^{-1}, for OER to occur. These findings imply that OER occurs at similar places along the Ni–Fe–O_x interface and that the Ni—Fe_2O_3 contact plays a significant role as the OER active site. Furthermore, it is also worth noting that the presence of metallic Ni allows for fast electron transit within the interface, which is necessary for successful electrocatalysis. Aside from the excellent OER performance, the exfoliated Ni–Fe–O_x demonstrated great stability with almost constant potential after 10 h of electrolysis at a current density of 10 mA cm^{-2}. This work confirms Ni–Fe–O_x is a promising, highly efficient and cost-effective OER catalyst for AEM electrolysis.

Keywords: oxygen evolution reaction; Ni–Fe–O_x; anion exchange membrane electrolysis; stability; non-noble metal

Citation: Vincent, I.; Lee, E.-C.; Kim, H.-M. Highly Active Ni–Fe Based Oxide Oxygen Evolution Reaction Electrocatalysts for Alkaline Anion Exchange Membrane Electrolyser. *Catalysts* **2022**, *12*, 476. https://doi.org/10.3390/catal12050476

Academic Editors: Sabrina Campagna Zignani, José Joaquín Linares León and Vincenzo Baglio

Received: 7 December 2021
Accepted: 20 April 2022
Published: 23 April 2022

1. Introduction

Low-temperature water electrolysis is a cutting-edge technology for the long-term production of hydrogen from renewable energy sources [1]. In power-to-gas operations, this technology provides adequate energy storage and grid-balancing utility [2,3]. Low-temperature water electrolysis has several advantages, including high efficiency, high product purity, stable output, the possibility of large-scale production, and the capacity to include renewable energy as a power source [4]. The conventional well-known low-temperature electrolysis technologies are proton exchange membrane (PEM) and alkaline water electrolysis [5]. The traditional PEM electrolysis necessitates the use of costly platinum metal group catalysis and an expensive Nafion membrane [6]. On the other hand, though mature alkaline electrolysis allows for the use of a less expensive catalyst, it has difficulty maintaining differential pressure when connected to renewable energy resources [7]. Recently, researchers developed anion exchange membrane (AEM) water electrolysis, a third-generation water electrolysis method that combines the advantages of both traditional PEM and alkaline electrolysis [8]. As with alkaline electrolysis, AEM electrolysis technology employs low-cost catalytic materials and a solid polymer electrolyte design, as does PEM electrolysis technology [9].

In AEM electrolysis, the oxygen evolution reaction (OER) and hydrogen evolution reaction (HER) are pair electrochemical reactions for dividing water to generate oxygen and hydrogen, respectively [10]. The current benchmark electrolyzer uses a RuO_2/IrO_2 anode and Pt-based cathode to accelerate OER and HER [11]. From the standpoint of commercialization, it is not only the high cost of noble metal elements that produce economic pressure but also the additional costs incurred as a result of the complexity of making diverse anode–cathode materials and probable cross-contamination [12]. Therefore, the creation of a universally active water-splitting catalyst based on earth-abundant minerals is of critical importance and represents a substantial innovation [13].

The OER suffers from significant overpotential losses when compared to the HER and has consequently been the target of numerous research efforts [14]. Reactions (1)–(5) offer an example of a standard OER process in alkaline media; however, alternative hypothesized or commonly employed mechanisms have been documented [15–17].

$$4OH^- \rightarrow O_2(g) + 2H_2O(l) + 4e^- \quad (1)$$

$$M + OH^- \rightarrow MOH^- + e^- \quad (2)$$

$$MOH + OH^- \rightarrow MO + H_2O(l) + e^- \quad (3)$$

$$MO + OH^- \rightarrow MOOH + e^- \quad (4)$$

$$MOOH + OH^- \rightarrow M + O_2(g) + H_2O(l) + e^- \quad (5)$$

Reactions (2)–(5) reflect a four-step process that describes the OER in general. These reactions illustrate a general OER process in which each step can be adjusted depending on the catalyst under consideration. Reaction (2) involves the generation of M-OH by one-electron oxidation of hydroxide anions adsorbed on the catalyst active site (M; may not always refer to a metal atom/site). After removing a pair of protons and an electron, M-OH turns into M-O in Reaction (3). Then, there are two alternative avenues for O_2 generation. Reaction (4) describes the initial step, in which two M-O species recombine to generate the O_2 molecule and two free M active sites. Reaction (5) describes the second mechanism, in which M–OOH is formed after merging with hydroxyl anion by one-electron oxidation (Reaction (4)). Following that, another proton-coupled electron transfer step occurs, yielding the O_2 molecule and the first active site (Reaction (5)) [18].

Because, since the OER is a four-electron transfer process requiring large overpotentials, so the efficiency of electrochemical water-splitting suffers from the sluggish kinetics of OER [19–21]. As a result, it is highly desirable to investigate active OER electrocatalysts in order to lower the energy barrier. In general, a noble metal such as Pt, an Ir-based catalyst, has been used to reduce the overpotential of the sluggish reaction. When OER occurs in an alkaline medium, the loading of noble metal catalysts can be decreased or eliminated entirely.

Transition-metal oxides (e.g., Co_3O_4, Fe_2O_3, Mn_3O_4, NiO, etc.) have received increasing interest as possible alternatives to noble metal catalysts due to their earth abundance and intrinsic stability in alkaline solutions [22–24]. Ni–Fe–O_x, in particular, has received extensive research since it is well-known as one of the most active OER electrocatalysts for alkaline water electrolysis [23,25–27]. While it is widely accepted that Fe plays an important role in increasing intrinsic activity, the effect of Fe on improved OER kinetics is still being debated. Many distinct mechanistic ideas have been offered in this regard. In theory, Fe inclusion can boost the conductivity of metal oxides (Co and Ni), which act as a scaffold for Fe active sites [28]. Surface-interrogation scanning electrochemical microscopy and Mössbauer spectroscopy were recently used to demonstrate the in situ production of Fe^{4+} in Ni–Fe oxide during the OER process [29–31]. Many studies have demonstrated that iron (Fe) combined with Ni produces some of the best OERs [32–34]. Some ascribe the rise in OER activity to the addition of the Fe active site [35]. For example, when more than 4.7% Fe was incorporated into NiFe-layered double hydroxide materials, the active site of the catalyst changed from Ni to Fe, boosting the catalyst's turnover frequency 20–200 fold [36].

Therefore, there is little doubt that the synergistic action of Ni and Fe contributes to superior OER activity when compared to pure nickel or iron oxide [37–39]. Calculations based on density functional theory (DFT) have also been used for (Ni,Fe)NiOOH systems for OER [40]. The (Ni,Fe)OOH system was discovered to be bi-functional, with both Ni and Fe working in synergy to catalyze the OER; Fe^{4+} helps create an active O radical species, while Ni^{4+} subsequently catalyzes O–O coupling, demonstrating that each metal helps with elemental phases of the OER mechanism [41,42]. Unfortunately, there are still no effective procedures for correctly evaluating catalysts on the substrate, as it is used as an anode in AEM electrolysis, which poses a challenge in quantifying and comparing the catalyst active area and performance.

In this present work, we find the OER activity of the Ni–Fe–O_x catalysts coated on the stainless steel surface as it is used in AEM electrolysis. The performance and stability of the Ni–Fe–O_x were evaluated in a three-electrode setup using cyclic voltammetry, electrochemical impedance spectroscopy, linear sweep voltammetry (LSV), and Tafel plots to further analyze the anode properties. Moreover, we find the performance of Ni–Fe–O_x as an anode catalyst in the whole AEM electrolyser for real-time applications.

2. Results and Discussion

2.1. Oxygen Evolution Reaction (OER)

We then investigated the OER performance of Ni–Fe–O_x supported on stainless steel fiber substrate, because of its excellent electrochemical properties, such as corrosion resistance against OER, electrical conductivity, a three-dimensional porous structure, and high mechanical strength [43]. Figure 1 depicts the results of the cyclic voltammetry studies, which demonstrate the obtained voltages for Ni–Fe–O_x and pure Ni. The oxidation and reduction characteristics are shown in Figure 1. Oxidation occurs at 1.52 V for Ni–Fe–O_x while reduction occurs at 1.41 V. For pure Ni, oxidation occurs at 1.45 V and reduction occurs at 1.37 V. At an over potential of 1.52 V, the maximum absorption of ions exhibited a high current density of 12 mA cm^{-2} for Ni–Fe–O_x. The pure Ni, on the other hand, demonstrated a current density of 2.5 mA cm^{-2} at a potential of 1.45 V. The difference in absorbed current density was 5.5 times less than that of Ni–Fe–O_x.

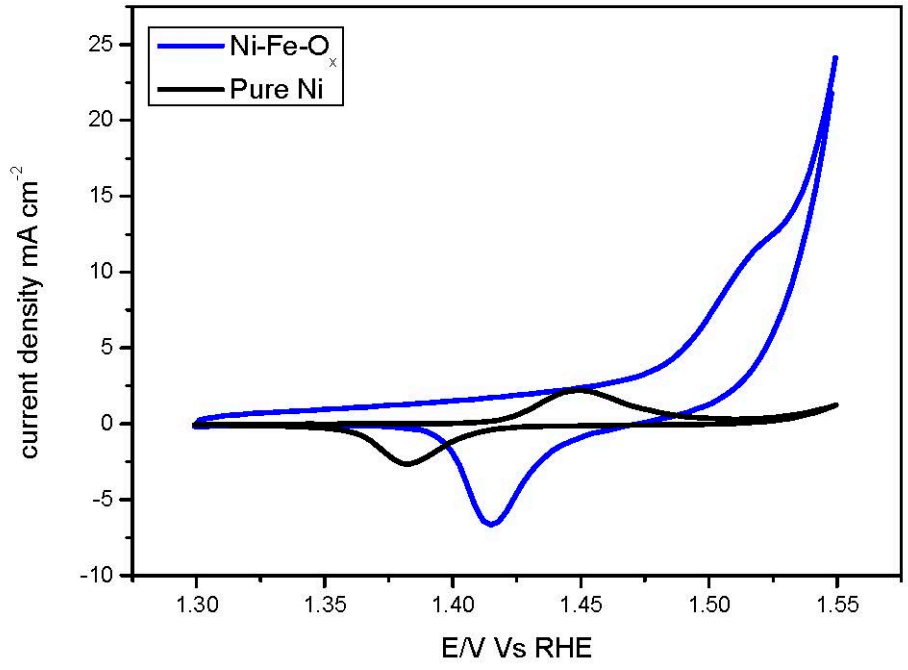

Figure 1. Cyclic voltammograms of Ni–Fe–O_x during the potential cycle between 1.3 and 1.55 V vs. RHE in 1 M KOH.

The LSV for Ni–Fe–O_x and pure Ni is shown in Figure 2 with a scan rate of 20 mV s^{-1} from 1.3 to 1.55 V. The OER began at roughly 1.52 V and then abruptly grew until 1.55 V, whereas the OER for pure Ni began at 1.4 V and then sharply increased. At 1.55 V, the obtained current density was 22 mA cm^{-2}, demonstrating superior performance over the non-noble metal electrocatalyst. The pure Ni, on the other hand, demonstrated a current density of 4.1 mA cm^{-2} at a potential of 1.55 V. The performance of Ni–Fe–O_x is five times that of pure Ni.

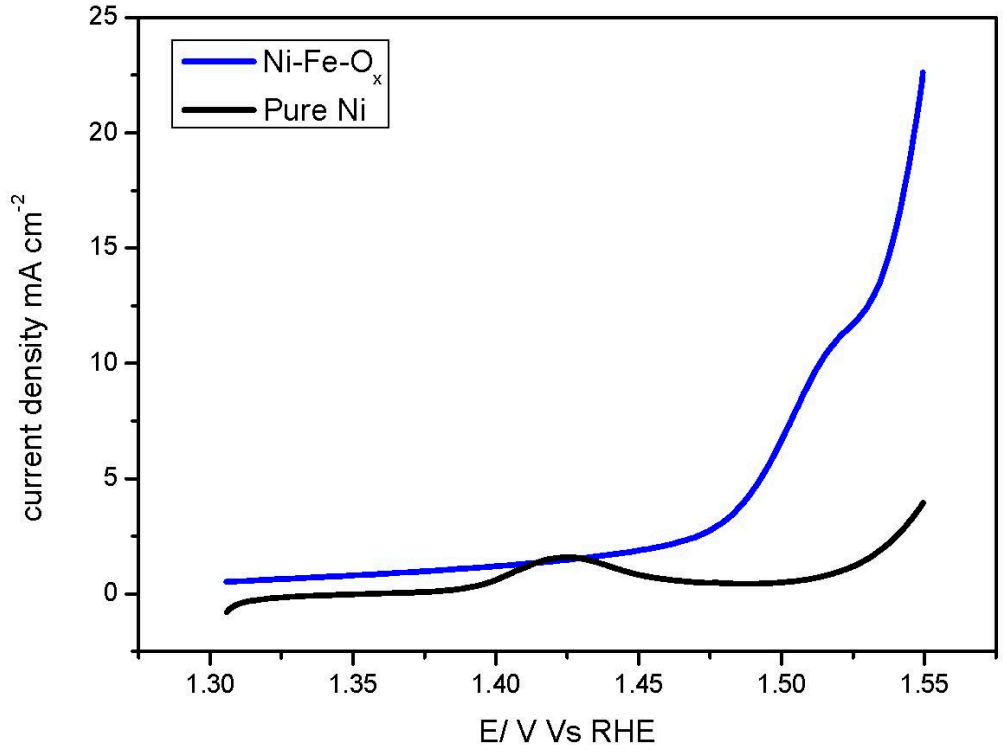

Figure 2. LSV of Ni–Fe–O_x as an OER electrocatalyst: from 1 to 2.2 V at 20 mV s^{-1} in 1 M KOH.

Importantly, Figure 2 indicates that in the Ni–Fe–O_x arrangement, the Ni oxidation peak prior to the initiation of OER was greatly inhibited. The oxidation peak corresponds to Ni oxidation from low valence states (Ni0, Ni^{2+}) to high valence states (Ni^{3+} or Ni^{4+}), the latter of which is thought to be active sites for OER [44,45]. The significantly lower Ni oxidation peak found in comparison to Ni Ni/Fe and Ni–Fe–O_x (Figure 2) shows that OER active sites are already present in the Ni–Fe–O_x, rather in operando generated. Consequently, if the potential could be decreased by 0.1 V for OER, the SS would be comparable to the best performing substrate for Ni–Fe–O_x, the full water-splitting reaction. These findings imply that both OER occur at similar places along the Ni–Fe–O_x interface. It is also worth noting that the presence of metallic Ni allows for fast electron transit within the nanoparticle, which is necessary for successful electrocatalysis.

Figure 3 depicts the Tafel slopes, showing the results for both the Ni–Fe–O_x and pure Ni electrodes. The slopes between the obtained cell voltages and logarithmic current density were drawn and calculated. The computed Tafel slope for the Ni–Fe–O_x electrode was 97 mV dec^{-1}, and a comparable value has already been reported in the literature [46]. The OER displayed two distinct Tafel zones. The first Tafel slope is related to the OER, whereas the second slope may be related to the oxide surface state. Despite the fact that the Tafel slopes value is lower than pure Ni, however, this is greater than the usual Ir and Pt catalyst values of 55 and 60 mV dec^{-1} [47]. Figure 3 demonstrates that the linearity of the curve is also maintained at high j, showing that the catalyst has fast electron transfer and mass transport properties [48].

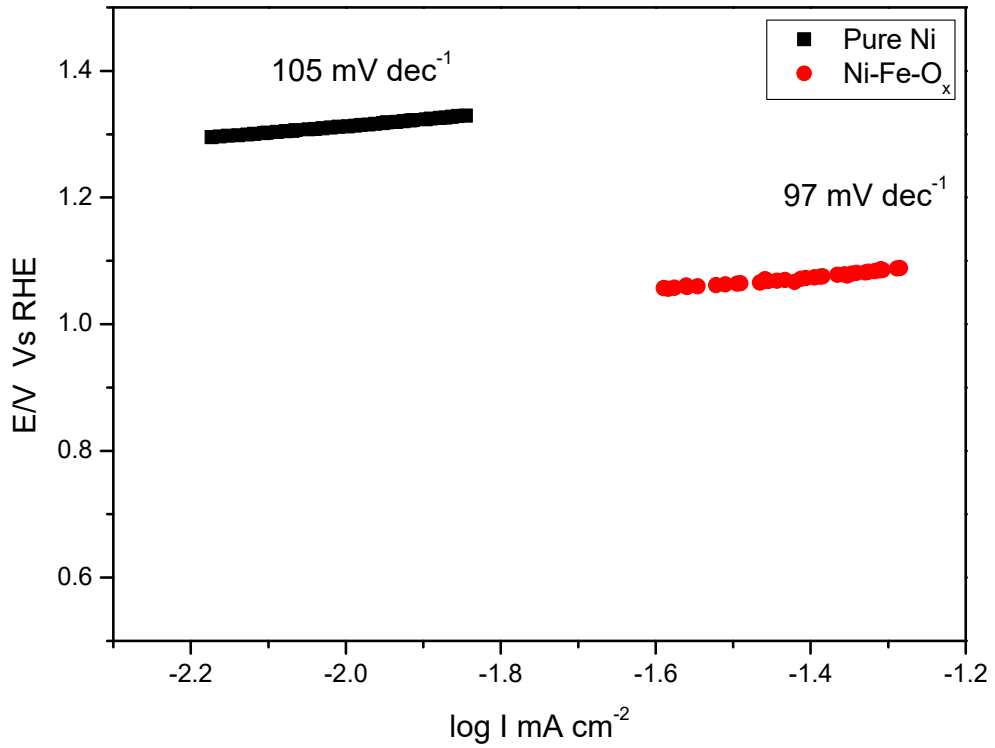

Figure 3. Tafel plots for the Ni–Fe–O_x and pure Ni catalysts in 1 M KOH.

2.2. Preliminary Durability in Oxygen Evolving Currents

In addition to OER activity, the catalyst's long-term stability over time is another important parameter to evaluate. Ni–Fe–O_x catalysts were tested by chronopotentiometry for 10 h and by the electrochemical impedance spectroscopy (EIS) method. The long-term stability of the electrocatalyst was confirmed by the chronopotentiometry (CP) of the Ni–Fe–O_x (Figure 4) at 10 mA cm^{-2} for 10 h. The sustained current applied to the catalyst electrode almost did not change the polarization curve, indicative of almost no change in charge transfer and reaction kinetics. Moreover, the cyclic stability of the catalyst was tested using cyclic voltammetry. The 1st and 1000th cycles were compared. In addition, no significant change was discovered. The before and after stability examination of EIS is shown in Figure 5, the measurement frequency range being from 100 to 0.1 Hz. The EIS was obtained under the overpotential condition of 1.6 V. The equivalent circuit model is shown as an inset of Figure 5, which exhibits ohmic resistance (Rs), charge-transfer resistance (Rct), and two constants. All of the EIS curves were composed of perfect semicircles. Before the stability test, the Rct of Ni–Fe–O_x was 1.178 Ω, and after the stability examination, the (Rct) became (1.272 Ω). Likewise, the charge-transfer resistances before and after stability examination were 0.733 and 0.545 Ω, indicating that Ni–Fe–O_x has a slower interface charge-transfer process. The semicircle of the Nyquist plot for the Ni–Fe–O_x sample increased after CP testing, indicating decreased charge-transfer abilities. In addition, the slight increase in the Tafel slope suggests a little retardance of reaction kinetics. Note that even after the long-term electrical operation, the Tafel slope of the Ni–Fe–O_x catalyst was still smaller than those of the initial values electrodes. This could be an indication of initial Fe dissolution from the sample with a higher starting iron content. This performance of the SS as a substrate is comparable to other highly efficient bi-functional nano-sized electrocatalysts adhered to high surface area 3D electrodes, and only slightly below the most efficient nano-sized bi-functional electrocatalysts thus far.

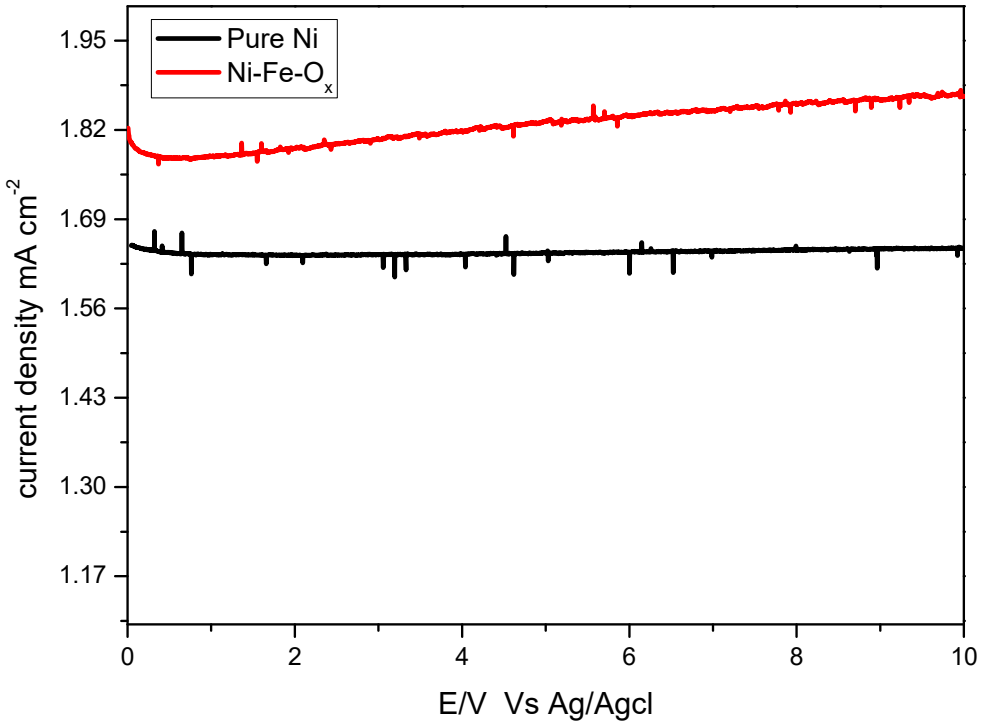

Figure 4. Chrono-potentiometric test of Ni–Fe–O_X alloy as an OER electrocatalyst at 1.6 V vs. RHE in 1 M KOH.

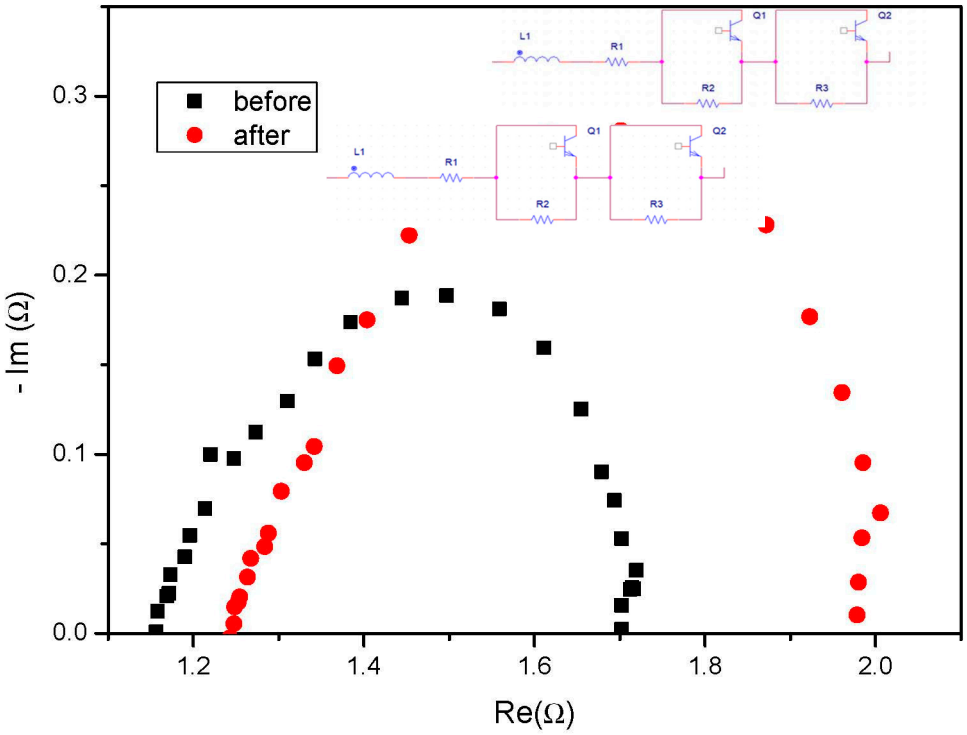

Figure 5. Stability determination from the Nyquist plots of the EIS measurements (from 100 kHz to 1 MHz) before and after 100 h.

2.3. Effect of Temperature on Electrochemical Analysis

The effect of temperature changes on Ni–Fe–Ox electrochemical performance was investigated. The effect of temperature on the electrochemical performance of the Ni–Fe–Ox was studied using cyclic voltammetry (CV) and electrochemical impedance spectroscopy

(EIS), which is shown in Figure 6a,b. CV, LSV, and EIS results show that as the operating temperature rises, electrochemical performance improves, with an increase in capacitance and a decrease in resistance.

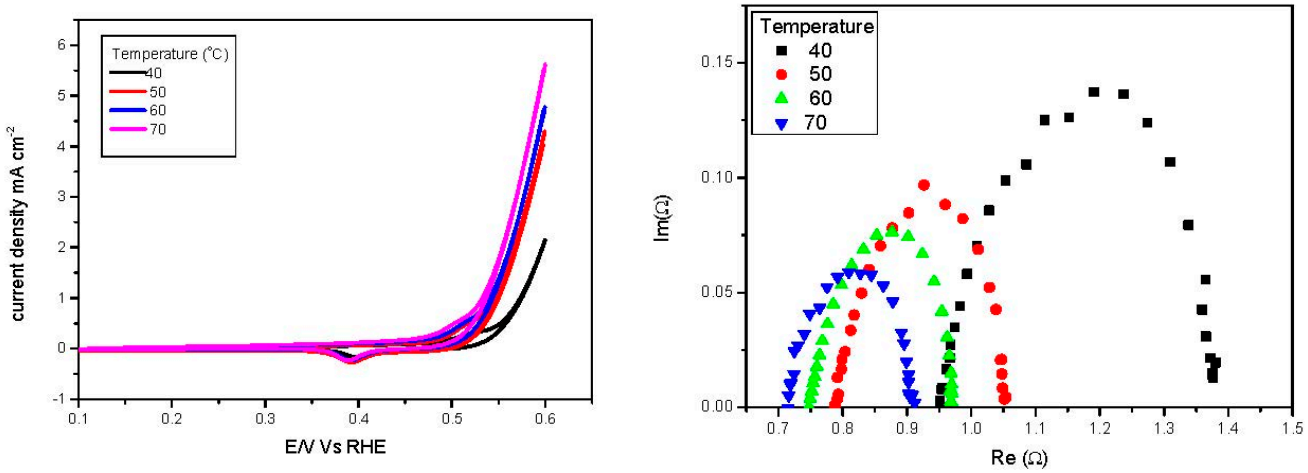

Figure 6. Effect of temperature on electrochemical performances (**a**) CV (**b**) EIS.

2.4. Performance and Stability of Ni–Fe–Ox Catalyst on AEM Electrolyser

Further, Ni–Fe–O_x catalyst was tested in the whole AEM electrolysis cell to find out its performance. Here, Ni–Fe–O_x and Ni–Fe–Co were used as both the anode and cathode in a whole cell water electrolyzer. A sustainion membrane was used as an AEM. The processes for making the MEA and the electrolysis setup were adapted from our earlier work [10]. The polarization curve of the Ni–Fe–O_x cell was recorded and compared to the cell constructed using benchmark noble metal catalysts, 20% Ir/C (OER) and 20% Pt/C (HER). Figure 7 shows the performance and stability of AEM electrolysis. The Ni–Fe–O_x cell exhibits a slightly lower performance compared to the Ir/C | | Pt/C cell. [49] The obtained cell voltage of Ni–Fe–O_x | |Ni–Fe–Co

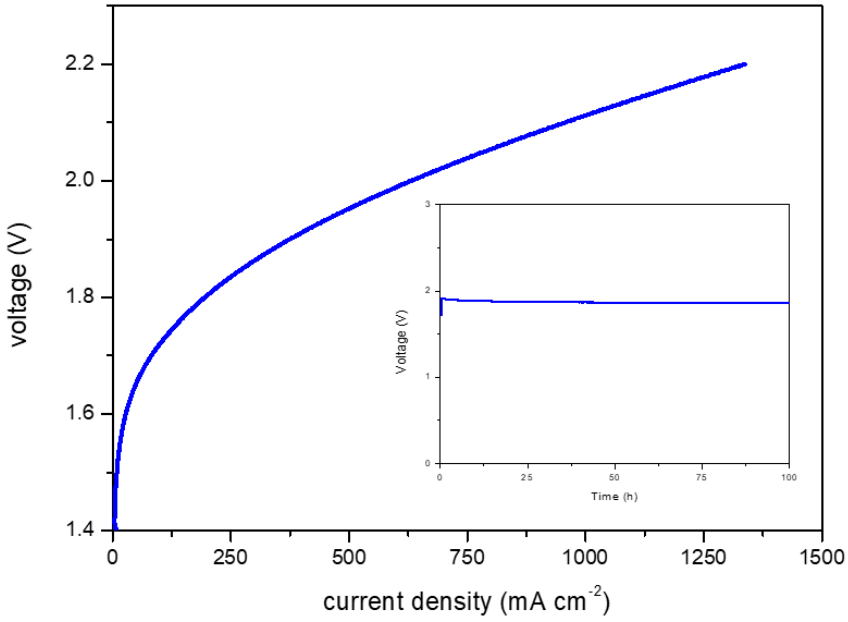

Figure 7. Performance and stability AEM electrolysis by using Ni–Fe–O_x–SS anode for 1 M KOH.

The electrolysis cell at 500 mA cm^{-2} was 1.98 V for 1 M KOH, whereas in the Ir/C | | Pt/C cell at 500 mA cm^{-2}, it was 1.60 V. The energy efficiency of the Ni–Fe–O_x cell was calculated to be 74.7%. The Ni–Fe–O_x | |Ni–Fe–Co also shows excellent stability during the 100 h bulk water electrolysis at j = 500 mA cm^{-2}. There was no evidence of severe deterioration of the catalytic layer or the membrane. Furthermore, an accelerated degradation test (ADT) was performed by repeatedly switching the polarity of the electrode to show the Ni–Fe–O_x electrochemical stability against power outages. The electrolysis current was varied between 100 mA cm^{-2} (OER) and −100 mA cm^{-2} (HER) in this experiment, and the Ni−Fe−O_x electrode was anodized for 600 s before switching to HER, and vice versa. The stable potential response throughout the 4200 s ADT shows the extraordinary stability of Ni−Fe−O_x as a reversible, bi-functional catalyst for water electrolysis under intermittent circumstances.

3. Experimental Methods

3.1. Electrode Fabrication

The homogeneous catalyst ink solution was made by combining de-ionized water, ionomer (Sustainion® XB-7, Dioxide Material, Boca Raton, FL, USA), and catalyst powder Ni–Fe–Ox (particle diameter of 0.5 mm), which was sonicated with ice for 15 min. The isopropyl alcohol was then added and sonicated for 10 min with ice. The slurry was then ultrasonicated for 10 min with ice using an ultrasonic probe (Branson Digital Sonifier Model 102 °C). It is assured that no aggregation was observed in the homogenous ink. The homogeneity of ink formulation is critical for achieving consistent results. The anode and cathode catalyst ink was brushed onto the surface of the stainless steel (SS) (80–110 ppi); American Elements, USA. The gas diffusion electrodes (GDE) were dried at 80 °C for 2 h. Simultaneously, the anode GDE was sintered for 30 min at 340 °C and the cathode GDE was sintered for 2 h at 300 °C. The OER and HER catalyst loadings were 5 mg_{cat} cm^{-2}, respectively. The anode and cathode were Ni–Fe–Ox and Ni–Fe–Co coated in Ni foam. The catalyst was loaded at a rate of 5 mg_{cat} cm^{-2}.

3.2. Electrochemical Characterization of Electrodes

The electrodes for the OER were investigated using a standard three-electrode electrochemical glass cell. Each compartment received a working, counter, and reference electrode. The manufactured anodes or cathodes served as direct working electrodes for the OER. Moreover, 1 cm^2 of electroactive surface area A platinum wire served as the counter electrode and an Ag/AgCl reference electrode served as the reference electrode. It was, however, converted back to RHE. The experimentally obtained potentials vs. Ag/AgCl were transformed to the reversible hydrogen electrode (RHE) scale using the Nernst equation:

$$E_{RHE} = E_{Ag/AgCl} + 0.059\ pH + Eo_{Ag/AgCl} \quad (6)$$

where E_{RHE} is the converted potential vs. RHE, $Eo_{Ag/AgCl}$ = 0.1976 at 25 °C, and $E_{Ag/AgCl}$ is prior to the trials; the working electrode surface was cleaned with ethanol and ultra-pure water. The studies were carried out at 40 °C with 1 M KOH. All tests were run with the EC labs software and the Bio-Logic potentiostat/galvanostat (Bio-Logic Science Instruments, Seyssinet, France).

3.3. Electrochemical Testing and Pretreatment

A series of tests were carried out to properly evaluate the OER activity of the synthesized materials. First, to calculate the ohmic losses of the system, potentiostatic electrochemical impedance spectroscopy (EIS) experiments were carried out around the OCP of each electrode using a sinus amplitude of 5 mV from 100 to 0.1 Hz. Then, to pretreat the electrode before OER testing, chronopotentiometry (CP) experiments were carried out at −1.3 V for 5 min and then at −1.8 V for 10 min. To evaluate the OER, cyclic voltammetry (CV) experiments were done between 1.1 and 1.8 V vs. RHE for 10 cycles at 25 mV s^{-1}, then, linear sweep voltammetry (LSV) experiments were done between 1.3 and 1.8 V vs. RHE for

1 sweep at 1 mV s^{-1}. Cycle 10 of the CVs is reported unless otherwise indicated. To test the preliminary electrode durability and mechanical integrity of the best performing electrodes, the CVs mentioned above were repeated for 300 cycles and chronopotentiometry (CP) measurements were done at 10 mA cm^{-2} for 10 h. Note that all presented currents were normalized using the geometric surface area of the electrode.

4. Summary

In this study, the Ni–Fe–O_x catalyst was studied as an active oxygen evolution reaction catalyst for applications in AEM electrolysis. The performance and stability were compared with the pure Ni and conventional Ir/Pt electrocatalysts. The performance of Ni–Fe–O_x is three times that of pure Ni. These findings imply that both OERs occur at similar places along the Ni–Fe–O_x interface. It is also worth noting that the presence of metallic Ni allows for fast electron transit within the nanoparticle, which is necessary for successful electrocatalysis. Stability results indicate that the Ni–Fe–O_x catalyst is, overall, the most stable material. The performance of the Ni–Fe–O_x as an OER catalyst on the AEM electrolysis is satisfactory, however, is still lower than the conventional PEM electrolysis. Overall, Ni–Fe–O_x catalysts in this study show OER activity; and excellent stability. This Ni–Fe–O_x catalyst shows good promise for highly active anodes in AEM water electrolysis.

Author Contributions: I.V. conceived and designed the experiments; H.-M.K. directed the project; I.V. and E.-C.L. performed the experiments; I.V. wrote the paper. All authors discussed the results and commented on the manuscript. All authors have read and agreed to the published version of the manuscript.

Funding: This research was funded by Foundation of Korea (NRF) grant number 2019H1D3A2A02102994. And the APC was funded by 2019R1I1A3A0305044112.

Acknowledgments: This work was supported by the Brain Pool Program through the National Research Foundation of Korea (NRF) funded by the Ministry of Science and ICT (grant number: 2019H1D3A2A02102994), and was supported by a Basic Science Research Program through the (NRF) funded by the Ministry of Education (2019R1I1A3A0305044112).

Conflicts of Interest: The authors declare no conflict of interests.

References

1. Schalenbach, M.; Zeradjanin, A.R.; Kasian, O.; Cherevko, S.; Mayrhofer, K.J.J. A perspective on low-temperature water electrolysis—Challenges in alkaline and acidic technology. *Int. J. Electrochem. Sci.* **2018**, *13*, 1173–1226. [CrossRef]
2. Blanco, H.; Faaij, A. A review at the role of storage in energy systems with a focus on Power to Gas and long-term storage. *Renew. Sustain. Energy Rev.* **2018**, *81*, 1049–1086. [CrossRef]
3. Ajiwibowo, M.W.; Darmawan, A.; Aziz, M. A conceptual chemical looping combustion power system design in a power-to-gas energy storage scenario. *Int. J. Hydrogen Energy* **2019**, *44*, 9636–9642. [CrossRef]
4. Park, J.; Kang, Z.; Bender, G.; Ulsh, M.; Mauger, S.A. Roll-to-roll production of catalyst coated membranes for low-temperature electrolyzers. *J. Power Sources* **2020**, *479*, 228819. [CrossRef]
5. Ayers, K.; Danilovic, N.; Ouimet, R.; Carmo, M.; Pivovar, B.; Bornstein, M. Perspectives on Low-Temperature Electrolysis and Potential for Renewable Hydrogen at Scale. *Annu. Rev. Chem. Biomol. Eng.* **2019**, *10*, 219–239. [CrossRef] [PubMed]
6. Lee, B.; Heo, J.; Kim, S.; Sung, C.; Moon, C.; Moon, S.; Lim, H. Economic feasibility studies of high pressure PEM water electrolysis for distributed H2 refueling stations. *Energy Convers. Manag.* **2018**, *162*, 139–144. [CrossRef]
7. Zeng, K.; Zhang, D. Recent progress in alkaline water electrolysis for hydrogen production and applications. *Prog. Energy Combust. Sci.* **2010**, *36*, 307–326. [CrossRef]
8. Vincent, I.; Bessarabov, D. Low cost hydrogen production by anion exchange membrane electrolysis: A review. *Renew. Sustain. Energy Rev.* **2018**, *81*, 1690–1704. [CrossRef]
9. Vincent, I.; Lee, E.-C.; Kim, H.-M. Comprehensive impedance investigation of low-cost anion exchange membrane electrolysis for large-scale hydrogen production. *Sci. Rep.* **2021**, *11*, 293. [CrossRef]
10. Vincent, I.; Lee, E.-C.; Kim, H.-M. Highly cost-effective platinum-free anion exchange membrane electrolysis for large scale energy storage and hydrogen production. *RSC Adv.* **2020**, *10*, 37429–37438. [CrossRef]
11. Leng, Y.; Chen, G.; Mendoza, A.J.; Tighe, T.B.; Hickner, M.A.; Wang, C.-Y. Solid-State Water Electrolysis with an Alkaline Membrane. *J. Am. Chem. Soc.* **2012**, *134*, 9054–9057. [CrossRef] [PubMed]
12. Vincent, I.; Kruger, A.; Bessarabov, D. Development of efficient membrane electrode assembly for low cost hydrogen production by anion exchange membrane electrolysis. *Int. J. Hydrogen Energy* **2017**, *42*, 10752–10761. [CrossRef]

13. Das, A.; Ganguli, A.K. Design of diverse nanostructures by hydrothermal and microemulsion routes for electrochemical water splitting. *RSC Adv.* **2018**, *8*, 25065–25078. [CrossRef]
14. Dubouis, N.; Grimaud, A. The hydrogen evolution reaction: From material to interfacial descriptors. *Chem. Sci.* **2019**, *10*, 9165–9181. [CrossRef] [PubMed]
15. Liang, Q.; Brocks, G.; Bieberle-Hütter, A. Oxygen evolution reaction (OER) mechanism under alkaline and acidic conditions. *J. Phys. Energy* **2021**, *3*, 026001. [CrossRef]
16. Wang, S.; Lu, A.; Zhong, C.-J. Hydrogen production from water electrolysis: Role of catalysts. *Nano Converg.* **2021**, *8*, 4. [CrossRef]
17. Li, G.; Anderson, L.; Chen, Y.; Pan, M.; Chuang, P.-Y.A. New insights into evaluating catalyst activity and stability for oxygen evolution reactions in alkaline media. *Sustain. Energy Fuels* **2018**, *2*, 237–251. [CrossRef]
18. Plevová, M.; Hnát, J.; Bouzek, K. Electrocatalysts for the oxygen evolution reaction in alkaline and neutral media. A comparative review. *J. Power Sources* **2021**, *507*, 230072. [CrossRef]
19. Song, J.; Wei, C.; Huang, Z.F.; Liu, C.; Zeng, L.; Wang, X.; Xu, Z.J. A review on fundamentals for designing oxygen evolution electrocatalysts. *Chem. Soc. Rev.* **2020**, *49*, 2196–2214. [CrossRef]
20. Bao, W.; Xiao, L.; Zhang, J.; Jiang, P.; Zou, X.; Yang, C.; Hao, X.; Ai, T. Electronic and structural engineering of $NiCo_2O_4$/Ti electrocatalysts for efficient oxygen evolution reaction. *Int. J. Hydrogen Energy* **2021**, *46*, 10259–10267. [CrossRef]
21. Zhao, G.; Rui, K.; Dou, S.X.; Sun, W. Boosting electrochemical water oxidation: The merits of heterostructured electrocatalysts. *J. Mater. Chem. A* **2020**, *8*, 6393–6405. [CrossRef]
22. Wang, Y.; Yan, D.; El Hankari, S.; Zou, Y.; Wang, S. Recent Progress on Layered Double Hydroxides and Their Derivatives for Electrocatalytic Water Splitting. *Adv. Sci.* **2018**, *5*, 1800064. [CrossRef] [PubMed]
23. Long, X.; Li, J.; Xiao, S.; Yan, K.; Wang, Z.; Chen, H.; Yang, S. A strongly coupled graphene and FeNi double hydroxide hybrid as an excellent electrocatalyst for the oxygen evolution reaction. *Angew. Chem. Int. Ed.* **2014**, *53*, 7584–7588. [CrossRef] [PubMed]
24. Yu, J.; Cao, Q.; Li, Y.; Long, X.; Yang, S.; Clark, J.K.; Nakabayashi, M.; Shibata, N.; Delaunay, J.-J. Defect-Rich $NiCeO_x$ Electrocatalyst with Ultrahigh Stability and Low Overpotential for Water Oxidation. *ACS Catal.* **2019**, *9*, 1605–1611. [CrossRef]
25. Gong, M.; Li, Y.; Wang, H.; Liang, Y.; Wu, J.Z.; Zhou, J.; Wang, J.; Regier, T.; Wei, F.; Dai, H. An advanced Ni-Fe layered double hydroxide electrocatalyst for water oxidation. *J. Am. Chem. Soc.* **2013**, *135*, 8452–8455. [CrossRef]
26. Chen, D.; Qiao, M.; Lu, Y.; Hao, L.; Liu, D.; Dong, C.; Li, Y.; Wang, S. Preferential Cation Vacancies in Perovskite Hydroxide for the Oxygen Evolution Reaction. *Angew. Chem. Int. Ed.* **2018**, *57*, 8691–8696. [CrossRef]
27. Wang, Y.; Qiao, M.; Li, Y.; Wang, S. Tuning Surface Electronic Configuration of NiFe LDHs Nanosheets by Introducing Cation Vacancies (Fe or Ni) as Highly Efficient Electrocatalysts for Oxygen Evolution Reaction. *Small* **2018**, *14*, 1800136. [CrossRef]
28. Osgood, H.; Devaguptapu, S.V.; Xu, H.; Cho, J.; Wu, G. Transition metal (Fe, Co, Ni, and Mn) oxides for oxygen reduction and evolution bifunctional catalysts in alkaline media. *Nano Today* **2016**, *11*, 601–625. [CrossRef]
29. Chen, J.Y.C.; Dang, L.; Liang, H.; Bi, W.; Gerken, J.B.; Jin, S.; Alp, E.E.; Stahl, S.S. Operando Analysis of NiFe and Fe Oxyhydroxide Electrocatalysts for Water Oxidation: Detection of Fe^{4+} by Mössbauer Spectroscopy. *J. Am. Chem. Soc.* **2015**, *137*, 15090–15093. [CrossRef]
30. Yu, M.; Moon, G.-H.; Bill, E.; Tüysüz, H. Optimizing Ni-Fe Oxide Electrocatalysts for Oxygen Evolution Reaction by Using Hard Templating as a Toolbox. *ACS Appl. Energy Mater.* **2019**, *2*, 1199–1209. [CrossRef]
31. Goldsmith, Z.K.; Harshan, A.K.; Gerken, J.B.; Vörös, M.; Galli, G.; Stahl, S.S.; Hammes-Schiffer, S. Characterization of NiFe oxyhydroxide electrocatalysts by integrated electronic structure calculations and spectroelectrochemistry. *Proc. Natl. Acad. Sci. USA* **2017**, *114*, 3050–3055. [CrossRef] [PubMed]
32. Song, F.; Busch, M.M.; Lassalle-Kaiser, B.; Hsu, C.-S.; Petkucheva, E.; Bensimon, M.; Chen, H.M.; Corminboeuf, C.; Hu, X. An Unconventional Iron Nickel Catalyst for the Oxygen Evolution Reaction. *ACS Central Sci.* **2019**, *5*, 558–568. [CrossRef] [PubMed]
33. Spanos, I.; Masa, J.; Zeradjanin, A.; Schlögl, R. The Effect of Iron Impurities on Transition Metal Catalysts for the Oxygen Evolution Reaction in Alkaline Environment: Activity Mediators or Active Sites? *Catal. Lett.* **2021**, *151*, 1843–1856. [CrossRef]
34. Hunter, B.M.; Winkler, J.R.; Gray, H.B. Iron Is the Active Site in Nickel/Iron Water Oxidation Electrocatalysts. *Molecules* **2018**, *23*, 903. [CrossRef]
35. Ahmeda, J.; Alama, M.; Khan, M.M.; Alshehri, S.M. Bifunctional electro-catalytic performances of NiMoO4-NRs@RGO nanocomposites for oxygen evolution and oxygen reduction reactions. *J. King Saud Univ. Sci.* **2021**, *33*, 101317. [CrossRef]
36. Farhat, R.; Dhainy, J.; Halaoui, L.I. Oer catalysis at activated and codeposited nife-oxo/hydroxide thin films is due to postdeposition surface-fe and is not sustainable without fe in solution. *ACS Catal.* **2019**, *10*, 20–35. [CrossRef]
37. Friebel, D.; Louie, M.W.; Bajdich, M.; Sanwald, K.E.; Cai, Y.; Wise, A.M.; Cheng, M.-J.; Sokaras, D.; Weng, T.-C.; Alonso-Mori, R.; et al. Identification of highly active Fe sites in (Ni,Fe)OOH for electrocatalytic water splitting. *J. Am. Chem. Soc.* **2015**, *137*, 1305–1313. [CrossRef]
38. Liang, C.; Zou, P.; Nairan, A.; Zhang, Y.; Liu, J.; Liu, K.; Hu, S.; Kang, F.; Fan, H.J.; Yang, C. Exceptional performance of hierarchical Ni-Fe oxyhydroxide@NiFe alloy nanowire array electrocatalysts for large current density water splitting. *Energy Environ. Sci.* **2020**, *13*, 86–95. [CrossRef]
39. Wang, L.; Ge, X.; Li, Y.; Liu, J.; Huang, L.; Feng, L.; Wang, Y. Nickel enhanced the catalytic activities of amorphous copper for the oxygen evolution reaction. *J. Mater. Chem. A* **2017**, *5*, 4331–4334. [CrossRef]
40. Ullah, H.; Loh, A.; Trudgeon, D.P.; Li, X. Density functional theory study of NiFeCo trinary oxy-hydroxides for an efficient and stable oxygen evolution reaction catalyst. *ACS Omega* **2020**, *5*, 20517–20524. [CrossRef]

41. Sayler, R.I.; Hunter, B.M.; Fu, W.; Gray, H.B.; Britt, R.D. EPR Spectroscopy of Iron- and Nickel-Doped [ZnAl]-Layered Double Hydroxides: Modeling Active Sites in Heterogeneous Water Oxidation Catalysts. *J. Am. Chem. Soc.* **2019**, *142*, 1838–1845. [CrossRef] [PubMed]
42. Rosen, B.M.; Quasdorf, K.W.; Wilson, D.A.; Zhang, N.; Resmerita, A.-M.; Garg, N.K.; Percec, V. Nickel-catalyzed cross-couplings involving carbon-oxygen bonds. *Chem. Rev.* **2010**, *111*, 1346–1416. [CrossRef] [PubMed]
43. Schäfer, H.; Sadaf, S.; Walder, L.; Kuepper, K.; Dinklage, S.; Wollschläger, J.; Schneider, L.; Steinhart, M.; Hardege, J.; Daum, D. Stainless steel made to rust: A robust water-splitting catalyst with benchmark characteristics. *Energy Environ. Sci.* **2015**, *8*, 2685–2697. [CrossRef]
44. Suryanto, B.H.R.; Fang, T.; Cheong, S.; Tilley, R.D.; Zhao, C. From the inside-out: Leached metal impurities in multiwall carbon nanotubes for purification or electrocatalysis. *J. Mater. Chem. A* **2018**, *6*, 4686–4694. [CrossRef]
45. Klaus, S.; Cai, Y.; Louie, M.W.; Trotochaud, L.; Bell, A.T. Effects of Fe electrolyte impurities on Ni(OH)2/NiOOH structure and oxygen evolution activity. *J. Phys. Chem. C* **2015**, *119*, 7243–7254. [CrossRef]
46. Zhang, X.; Xu, H.; Li, X.; Li, Y.; Yang, T.; Liang, Y. Facile Synthesis of Nickel–Iron/Nanocarbon Hybrids as Advanced Electrocatalysts for Efficient Water Splitting. *ACS Catal.* **2016**, *6*, 580–588. [CrossRef]
47. De Carvalho, J.; Filho, G.T.; Avaca, L.; Gonzalez, E. Electrodeposits of iron and nickel-iron for hydrogen evolution in alkaline solutions. *Int. J. Hydrogen Energy* **1989**, *14*, 161–165. [CrossRef]
48. Xu, Z.; Ying, Y.; Zhang, G.; Li, K.; Liu, Y.; Fu, N.; Guo, X.; Yu, F.; Huang, H. Engineering NiFe layered double hydroxide by valence control and intermediate stabilization toward the oxygen evolution reaction. *J. Mater. Chem. A* **2020**, *8*, 26130–26138. [CrossRef]
49. Millet, P.; Mbemba, N.; Grigoriev, S.A.; Fateev, V.N.; Aukauloo, A.; Etiévant, C. Electrochemical performances of PEM water electrolysis cells and perspectives. *Int. J. Hydrogen Energy* **2011**, *36*, 4134–4142. [CrossRef]